Title
Comments on the electron-cloud effect in the LHC dipole bending magnets

Author
Furman, Miguel A.

Publication Date
1997-10-01

LBNL-40914/CBP Note 241

Comments on the Electron-Cloud Effect in the LHC Dipole Bending Magnets*

Miguel A. Furman

Center for Beam Physics
Accelerator and Fusion Research Division
Lawrence Berkeley National Laboratory, MS 71-259
University of California
Berkeley, CA 94720

October 17, 1997

Abstract

We have applied our simulation code "POSINST" to estimate the power deposition per unit length from the electron cloud hitting the walls of the vacuum chamber liner in a dipole bending magnet. We also present rough estimates for the electron-cloud instability growth rate.

1 Introduction.

It is becoming increasingly clear that the electron cloud that inevitably accompanies a positron beam has potentially serious detrimental effects for high-current, multibunch beams [1]. Recently Zimmermann [2] pointed out that such an effect is expected to arise in the LHC as well. We have applied our simulation code "POSINST," developed over the past two years to study the electron-cloud instability (ECI) for the PEP-II low-energy ring [3], to the LHC. We focus on the estimate of the power deposition on the vacuum chamber liner in a region inside a dipole bending magnet as the electrons in the cloud are successively kicked transversely back and forth by the beam. We also provide an estimate of the ECI growth rate.

In our simulation model the electron secondary emission process is described in a fair amount of detail, and the secondary emission yield (SEY), δ_t, involves many parameters. As a rough first step to obtain our estimates, we have taken the SEY parameters for the model embodied in POSINST from fits to experimental data obtained at SLAC for aluminum and TiN-coated aluminum [4], and we have scaled the peak value of δ_t so as to roughly correspond to copper, which coats the interior of the LHC liner.

Two other basic inputs to the simulation are the photoelectric quantum efficiency Y' and the photon reflectivity R. We assume, also as part of this rough first step, that $R \lesssim 1$. This assumption implies that the photons emitted by the protons will bounce many times inside the chamber before yielding photoelectrons. This multiple-bounce process has the effect of making the distribution of photoelectrons essentially uniform both transversely and longitudinally, thus simplifying the problem considerably by decoupling the beam-electron interaction from the geometrical details of the synchrotron radiation captured by the liner.

A key ingredient in the simulation is the computation of the electric field produced by the bunches and the space-charge force from the electrons in the cloud. In order to simplify the computation we make the assumption that the vacuum chamber liner cross-section, which is specified to be a circle with flattened top

*Work supported by the US Department of Energy under contract no. DE-AC03-76SF00098. To be published in the proceedings of the MBI-97 Workshop, KEK, Tsukuba, Japan, 15–18 July 1997.

and bottom [5], can be sensibly approximated by an elliptical shape. This approximation allows us to use the analytic expression for the electric field subject to perfect-conductor boundary conditions [6].

We also use a very simplified model of the LHC ring, as described below. In this model the ring consists of nothing but 1232 identical, evenly-spaced dipole bending magnets plus 1232 identical field-free sections that alternate with the magnets.

We present our simulation results in the form of plots of the power deposition per unit length *vs.* Y' for several chosen peak values of the SEY δ_t.

2 Model of photoelectron emission.

2.1 Definitions of the quantum efficiency.

A good approximate description of the photoelectric effect is the following: when a pulse of N_0 photons strikes the surface of a material, a certain number N_r is reflected elastically off the surface and the rest, $N_0 - N_r$, penetrates into the material. Of these, N_i yield N_e photoelectrons, and the rest, N_a, are absorbed and turn into heat. Figure 1 sketches the situation. We define the quantum efficiency Y to be the number

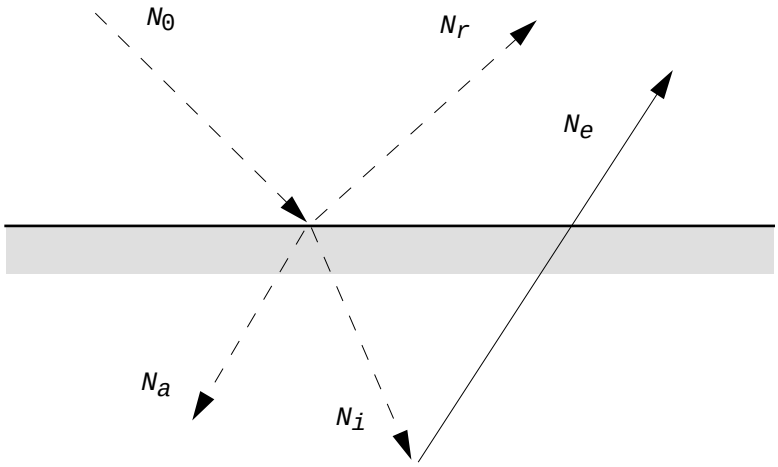

Figure 1: Sketch of the photoelectric effect. Dashed lines represent photons, solid line photoelectrons.

of photoelectrons generated per incident photon, thus

$$N_e \equiv Y N_0 \tag{2.1}$$

Similarly, we define the reflectivity R and the absorption coefficient A as

$$N_r \equiv R N_0, \qquad N_a \equiv A N_0 \tag{2.2}$$

These basic quantities Y, A and R depend strongly on the type of surface material, photon energy and angle of incidence.

An alternative definition of the quantum efficiency, which is more fundamental and directly relevant to the electron-cloud effect (but less convenient to measure directly), is the number of photoelectrons generated *per photon that penetrated the material*. If we call it Y', then it is given by

$$Y' = \frac{N_e}{N_0 - N_r} = \frac{Y}{1 - R} \tag{2.3}$$

This definition is more relevant to the problem at hand because it describes the total number of photoelectrons per photon that are generated anywhere downstream of the photon emission point. To see this, refer to Fig. 2 which sketches the fate of N_0 photons as they bounce inside a chamber. When these photons first strike the wall, they generate YN_0 photoelectrons. However, a fraction R of the photons are reflected at the surface and strike the wall further downstream, generating an additional RYN_0 photoelectrons. Similarly, a fraction R of these photons are reflected, and hit the chamber walls even further downstream, and so on, as sketched in Fig. 2. Thus the total number of photoelectrons generated is given by

$$N_{e,\mathrm{tot}} = YN_0(1 + R + R^2 + R^3 + \cdots) = \frac{Y}{1-R}N_0 = Y'N_0 \tag{2.4}$$

This calculation assumes that fluorescence can be ignored, a good approximation in the case of the LHC. It also assumes that the reflection process is specular, so that the incident-angle dependence of R and Y' is the same for all bounces.

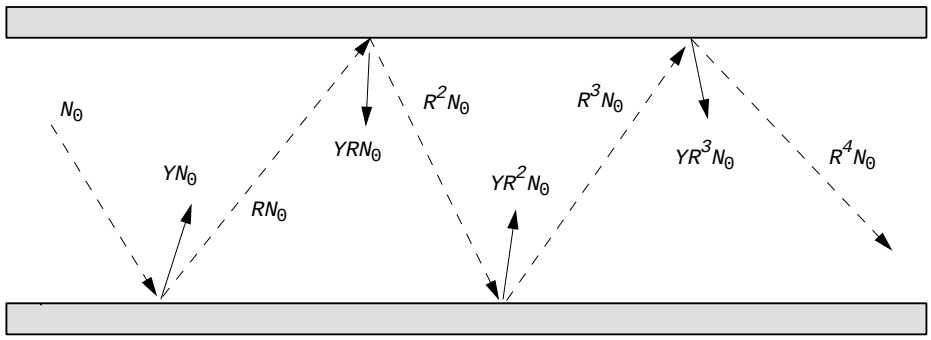

Figure 2: A initial pulse of N_0 photons strikes the wall of a closed vacuum chamber. Upon each bounce, some photoelectrons are generated and some photons are reflected.

3 Model for the LHC and photon spectrum.

The model beam is composed of identical, evenly-spaced bunches separated by a spacing $s_B = 7.48$ m with no gaps in the bunch train. We assume a bunch population $N_p = 1.05 \times 10^{11}$ protons per bunch, and average transverse rms beam sizes $\sigma_x = \sigma_y = 0.3$ mm and rms bunch length $\sigma_z = 7.7$ cm.

In our model we represent the cross-section of the vacuum chamber liner by an ellipse with semi-axes $a = 2.2$ cm and $b = 1.8$ cm, as sketched in Fig. 3. We also assume a simplified model of the ring and the beam, which consists of 1232 identical, evenly-spaced dipole bending magnets of length 14.2 m each, and 1232 field-free sections of length 7.44 m in between every pair of dipole magnets. The "half-cell" (the basic periodic unit of the ring) therefore has a length $L_u = 14.2 + 7.44 = 21.64$ m. These lengths add up to a model ring circumference $C = 1232 \times 21.64 = 26660.48$ m. The dipoles have a magnetic field $B = 8.4$ T, and the beam orbit through them has a radius of curvature $\rho = 2784.32$ m. The section of arc subtended by a dipole magnet is $\Delta\theta = 2\pi/1232 = 5.1 \times 10^{-3}$ rad.

For a beam energy $E = 7$ TeV, the critical energy of the synchrotron radiation from a proton traversing a dipole magnet is given by

$$E_{\mathrm{crit}} = \frac{3\hbar c}{2\rho}\,\gamma^3 = 44.1 \text{ eV} \tag{3.1}$$

where γ is the usual relativistic factor of the proton. Each proton generates, on average,

$$N_{\gamma/p} = \frac{5\alpha\gamma}{2\sqrt{3}}\,\Delta\theta = 0.4 \tag{3.2}$$

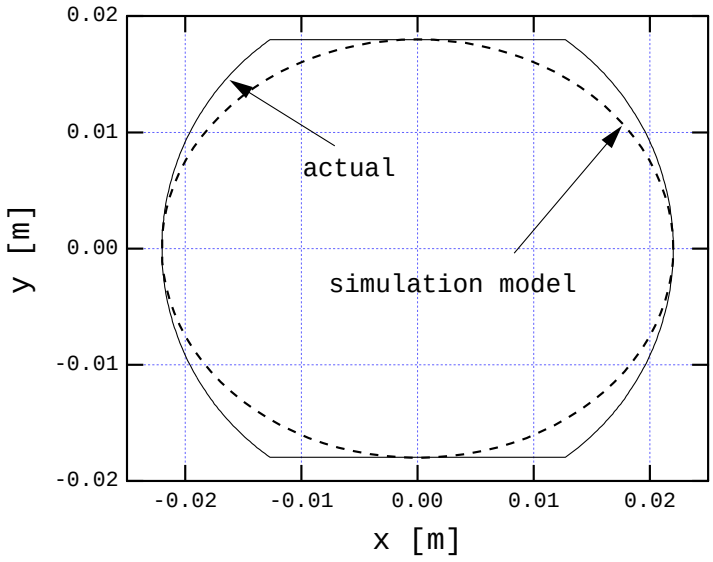

Figure 3: In our model, we replace the actual transverse cross-section of the LHC liner by the inscribed ellipse.

incoherent photons of all energies and directions upon traversing any given dipole bending magnet ($\alpha \simeq 1/137$ is the fine structure constant). Coherent photons can be completely neglected due to their very low energy.

3.1 Number of photoelectrons generated per bunch passage.

The number of photoelectrons generated in a given section of the ring per bunch passage is directly proportional to the average number of photons that strike the vacuum chamber wall of this section during such time. If $R \lesssim 1$, the photons will bounce many times inside the chamber downstream of their emission point and, as a result, they will get quite uniformly distributed both longitudinally (along the pipe) and transversely before they yield photoelectrons. As a result, the photoelectrons are also generated approximately uniformly. Consider a section of the vacuum chamber (either a dipole bending magnet, or a field-free section, or a portion thereof) whose length is L_s. Then the time-averaged number of photoelectrons generated in a time interval equal to the bunch spacing, s_B/c, in this section following the passage of a single proton through a bending magnet is

$$\bar{N}_{e/p} = Y' N_{\gamma/p} \frac{L_s}{L_u} \tag{3.3}$$

and the corresponding quantity per bunch (rather than per proton) is

$$\bar{N}_e = Y' N_{\gamma/p} N_p \frac{L_s}{L_u} \tag{3.4}$$

In addition to photoelectrons, there are electrons produced by beam ionization of the residual gas. For typical values of the residual gas pressure, temperature, and quantum efficiency one can show that the number of ionization electrons is several orders of magnitude smaller than photoelectrons, and hence can be completely ignored.

4 Secondary emission yield.

The generally-accepted picture of secondary emission is the following: when a current I_0 of electrons strikes the surface of a material, a certain portion I_e is reflected elastically off the surface, and the rest penetrates

into the material. Some of these electrons scatter from one or more atoms inside the material and are reflected back out (these are the so-called "rediffused" electrons); we call the corresponding current I_r. The rest of the electrons interact in a nontrivial (inelastic) way with the material and yield the so-called "true secondary electrons," whose current we call I_{ts}. The true secondaries typically dominate the SEY by far, except at low incident energies ($E_0 \simeq 30 - 50$ eV), where the elastic component is much more important.

The basic quantity used in the simulation program is the total yield δ_t, defined by

$$\delta_t = \frac{I_e + I_r + I_{ts}}{I_0} = \delta_e + \delta_r + \delta_{ts} \tag{4.1}$$

The details of the incident energy and angle dependence of these three components are described in more detail elsewhere [7]. As an example, figure 4 shows the curve for δ_t obtained by an approximate fit of experimental data for the SEY of aluminum obtained from measurements at SLAC [4].

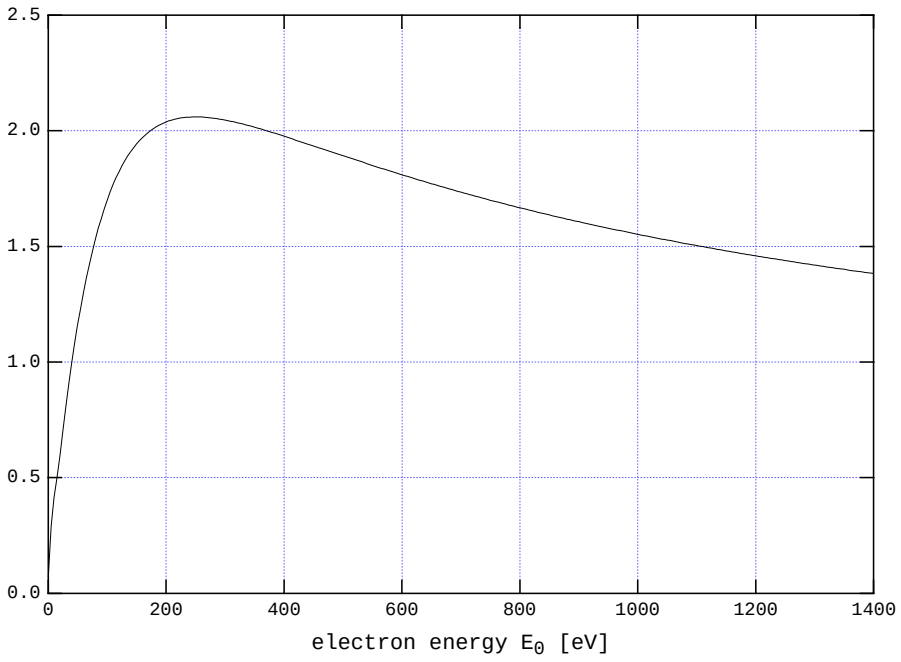

Figure 4: The total SEY δ_t of Al_2O_3 at normal incidence as a function of incident electron energy. This curve was obtained by fitting our model to experimental data [4] obtained at SLAC.

Experimentally, it is well-known that the true secondary electrons emitted from amorphous surfaces have a $\cos\theta$-distribution in angle, which is fairly independent of the primary incident angle θ_0. This is not quite true of the elastically reflected and rediffused electrons, which have more complicated angular distributions. However, we have carried out spot-checks that show that the results are fairly insensitive to the angular distribution. Therefore, for simplicity, we choose in our simulation a $\cos\theta$-distribution for all emitted electrons, regardless of the physical mechanism by which they were generated.

5 The transverse electric field.

For a relativistic bunch of N_p particles it can be shown that the longitudinal part of the electric field $\mathbf{E}$ vanishes, and the transverse part is proportional to the longitudinal (linear) charge density λ,

$$E_z = 0, \qquad \mathbf{E}_\perp = (E_x, E_y) = \lambda(s - ct)\mathbf{F}(x, y) \tag{5.1}$$

where $\mathbf{F}$ is a two-component vector with dimensions of 1/length that satisfies the two-dimensional transverse Poisson equation.

Since the field is effectively two-dimensional, it is natural to use complex notation to represent it [8]. Thus we define the "complex electric field,"

$$\mathcal{E} \equiv F_x + iF_y \tag{5.2}$$

which is really the electric field per unit linear charge density and not the electric field itself.

For an infinitely thin line of charge located at the point (x_0, y_0) inside an elliptical chamber of semi-axes (a, b), with $a > b$ and a along x, the solution of the transverse Poisson equation subject to perfect-conductor boundary conditions is most conveniently solved in elliptic coordinates (μ, ϕ), yielding [6]

$$\mathcal{E} = \frac{2}{\bar{z} - \bar{z}_0} + \frac{4}{g}\sum_{n=1}^{\infty} e^{-n\mu_1}\left[\frac{\cosh n\mu_0 \cos n\phi_0}{\cosh n\mu_1} + i\frac{\sinh n\mu_0 \sin n\phi_0}{\sinh n\mu_1}\right]\frac{\sinh n\bar{q}}{\sinh \bar{q}} \tag{5.3}$$

where the bar denotes complex conjugation; $z \equiv x + iy \equiv g\cosh q$ with $q \equiv \mu + i\phi$ being the elliptic coordinates in complex form of the point (x, y); $z_0 = x_0 + iy_0 = g\cosh(\mu_0 + i\phi_0)$; and where

$$g = \sqrt{a^2 - b^2}, \qquad \mu_1 = \tanh^{-1}\left(\frac{b}{a}\right) = \frac{1}{2}\log\left(\frac{a+b}{a-b}\right) \tag{5.4}$$

The first term in Eq.(5.3) represents the field from the "direct charge," and the summation is the contribution from the surface charges.[1] It is straightforward to show that the series converges whenever (x, y) is inside the chamber.

Now the transverse distribution of the beam is approximately gaussian with rms sizes σ_x, σ_y which are much smaller than the transverse dimensions of the chamber. At distances beyond a few σ's from the beam, the details of the transverse particle distribution are not important, and the surface charges become more and more important as the observation point approaches the walls of the chamber. Therefore in this region we approximate the field by that of a thin line of charge, Eq. (5.3). Near the beam the electric field from the surface charges is negligible so we can approximate the field by the direct component, given by the Bassetti-Erskine formula [9]. To simplify the calculation even further, we use the linearized form of this formula inside the $1-\sigma$ ellipse. In summary, for the field calculation in our simulation we use

$$\mathcal{E} = \begin{cases} \dfrac{2(\xi - \xi_0)}{\sigma_x + \sigma_y} & \text{for } |\xi - \xi_0| \le 1 \\ \text{Eq. (5.3)} & \text{for } |\xi - \xi_0| > 1 \end{cases} \tag{5.5}$$

where the bunch center is assumed to be at location (x_0, y_0), and we have defined $\xi = x/\sigma_x + iy/\sigma_y$ and $\xi_0 = x_0/\sigma_x + iy_0/\sigma_y$.

6 Beam-electron interaction.

For a nonrelativistic electron, the bunch-electron interaction is represented, in the impulse approximation, by the kick

$$\Delta p_x + i\Delta p_y = -\frac{e^2 N_p}{c}\,\mathcal{E} \tag{6.1}$$

It has been recently pointed out [10] that this approximation is not expected to be a good one for the LHC since the bunch length is roughly twice as long as the chamber is wide. The standard improvement to this approximation consists in "slicing" the bunch so that any given electron gets kicked several times during a bunch passage and adding up the effects from these kicks. It turns out, however, that, for nominal LHC

[1] It should be noted that the n-th term in the summation does *not* represent an image charge.

beam parameters, the impulse approximation is still roughly valid when used in the presence of a strong uniform magnetic field B provided it is modified according to [3]

$$\Delta p_x + i\Delta p_y = -\frac{e^2 N_p}{c}(S\mathcal{E}_x + i\mathcal{E}_y) \tag{6.2}$$

where we have assumed that the B field is along the y direction and where S is a "cyclotron phase suppression factor" given by

$$S = \int_{-\infty}^{\infty} dz\, \hat{\lambda}(z)\, e^{-i\omega z/c} \tag{6.3}$$

Here $\hat{\lambda}(z)$ is the longitudinal charge distribution of the bunch, normalized to unity, and $\omega = eB/mc$ is the cyclotron frequency of the electron in the field. For a gaussian bunch distribution, with $\hat{\lambda}(z) = e^{-(z/\sigma_z)^2/2}/\sqrt{2\pi}\sigma_z$, this yields

$$S = \exp\left(-\tfrac{1}{2}(\omega\sigma_t)^2\right) \tag{6.4}$$

where $\sigma_t = \sigma_z/c$. For the case of the LHC, the cyclotron frequency of a nonrelativistic electron in a dipole bending magnet is

$$\omega = \frac{eB}{mc} = 1.48 \times 10^{12} \quad \text{rad/s} \tag{6.5}$$

and therefore

$$S = 10^{-3.1\times 10^4} \tag{6.6}$$

which implies that the horizontal kick is wholly suppressed.

7 Space-charge forces.

Assuming a longitudinally uniform density of the cloud, we compute the space-charge forces from the electrons on themselves by using a square grid and adding up the electric field (5.3) from all the electrons at all grid points. We then compute the fields at the actual location of the electrons by using an area-weighted interpolation [11].

Typically we use a 5×5 mm grid cell, with spot checks using 1×1 mm. We compute the space-charge field once following a bunch passage, but we apply it on the electrons a certain number of times in between successive bunches, typically 4, with spot-checks to 8.

8 Calculation of the wake function and ECI growth rate.

For the calculation of the wake function we follow the conventions of Ref. [12]. Let Δp_y be momentum impulse experienced by the "trailing bunch" as it traverses a single section of length L_s keeping a fixed distance z behind the "perturbing bunch." Assuming that there are N_s such sections in the ring, their aggregate contribution to the dipole wake is given by

$$W_y(z) = -\frac{N_s L_s \bar{F}_y}{qQ\Delta y} = -\frac{cN_s}{(eN_p)^2} \cdot \frac{\Delta p_y}{\Delta y} \tag{8.1}$$

where $\bar{F}_y$ is the average force experienced by the trailing bunch as it traverses one section, namely $\bar{F}_y = \Delta p_y/\Delta t$ with $\Delta t = L_s/c$. Now, in the simulation, we compute Δp_y from the macroparticles that represent the electrons in the cloud. Therefore, the actual value for the wake function is obtained by replacing

$$\frac{\Delta p_y}{\Delta y} \to \frac{\Delta p_y}{\Delta y} \times \mathcal{F} \tag{8.2}$$

where $\mathcal{F}$ is the macroparticle-to-particle factor, discussed below.

As it turns out for the case of the LHC, the wake function is very short-range, *i.e.*, $|W(s_B)| \gg |W(ks_B)|$ for all $k \geq 2$. In this case, since the number of bunches M is $\gg 1$, a good estimate for the instability growth rate, which we call τ_0^{-1}, is given by [12]

$$\tau_0^{-1} \simeq \frac{ce^2 N_p}{4\pi E \nu_\beta} |W(s_B)| \tag{8.3}$$

where E is the beam energy and ν_β is the betatron tune. If the beam is not equally populated but has a gap, as is usually the case, the unstable modes do not grow exponentially in time if the range of the wake function is finite (*i.e.*, short compared with the length of the bunch train). In this situation the amplitude growth follows a power law rather than an exponential [12]. For example, in the simplest case, when the range of the wake function is one bunch spacing, the amplitude of the n-th bunch grows like

$$y_n(t) \propto (t/\tau_0)^{n-1} \tag{8.4}$$

where we take the convention that the head bunch is labeled $n = 1$. The important thing is that, in this formula, τ_0 is *the same quantity* given by Eq. (8.3). Since the amplitude of the trailing bunches in the train grows with a large power when $M \gg 1$, there is no practical difference between the beam-gap case and the uniformly-populated-beam case.

9 Simulation procedure.

Our program "POSINST" simulates the dynamics of the electron cloud and computes the effective wake function following the same ideas as in ref. [13]. The code simulates the cloud within a single specified section of the ring and evaluates, in addition to the wake function, various statistical quantities and spectra of the electron cloud.

The basic input to the simulation is the number of photoelectrons per bunch passage, $\bar{N}_e$, given by Eq. (3.4), which are represented by a *fixed number* of macroparticles, $N_{\rm phel}$. These are generated at every bunch passage at the walls of the section being simulated. They are distributed uniformly around the liner (both transversely and longitudinally), with a gaussian distribution in kinetic energy that peaks at 5 eV and has a width of 5 eV. The angles of the photoelectrons are generated with a $\cos\theta$-distribution where θ is the angle relative to the normal to the surface at the point of emission. These electrons are then kicked by successive bunches as they traverse the section. When the electrons collide at the chamber wall, they are either absorbed or create secondary electrons according to the SEY model described in Sec. 4. Space-charge effects are included in the motion of the electrons in the cloud.

We start the simulation by injecting a train of bunches into an empty vacuum chamber. We compute the dipole wake function by letting one bunch, say bunch number n, be displaced vertically from the equilibrium orbit by an amount Δy; this displaced bunch perturbs the electron cloud. We then measure the momentum kick Δp_y arising from this perturbation on bunches $n+1,\ n+2$, etc, which are themselves not displaced, and obtain the wake function from Eq. (8.1) for $z = 0,\ s_B,\ 2s_B$, etc.

In practice, one cannot simulate the electron cloud with a realistic number of particles, which is expected to be in the range $10^8 - 10^{10}$ per section, since this number is too large for present-day computers. Thus one resorts to simulating a much smaller number of representative particles, usually referred to as "macroparticles." In order to obtain quantitative results from the simulation which can be compared with a real machine, one must scale all electron-density-dependent quantities obtained from the simulation by a density factor $\mathcal{F}$, which can also be interpreted as the macroparticle-to-particle charge ratio, given by

$$\mathcal{F} = \frac{\text{number of electrons in reality}}{\text{number of electrons in the simulation}} \tag{9.1}$$

Neither the numerator nor the denominator in Eq. (9.1) is known a priori, so we need a more convenient expression to compute the density factor $\mathcal{F}$. Since the basic input value to our simulation is the number of

macro-photoelectrons per bunch passage, $N_{\rm phel}$, we can express $\mathcal{F}$ as

$$\mathcal{F} = \frac{\bar{N}_e}{N_{\rm phel}} \tag{9.2}$$

The numerator in this formula is the total number of real photoelectrons created in the section being simulated during a time interval equal to a bunch spacing, s_B/c, while the denominator is the corresponding number of macro-photoelectrons. Eqs. (9.2) and (9.1) are equivalent because the number of electrons in existence in the simulation (and in reality) is directly proportional to the number of photoelectrons.

10 Results for $R \lesssim 1$.

10.1 Development of the cloud.

As an example, we run a simulation in which $N_{\rm phel} = 10000$, with $Y' = 1$ and $\hat{\delta}_t = 1.3$. We choose a 5×5 mm grid for the space-charge calculation, and we divide the bunch spacing into 4 steps. Figure 5 shows the development of the electron cloud in a dipole bending magnet. One can see that an equilibrium is reached after ~ 8 bunch passages, at which point the average electron density stabilizes at $\sim 50\%$ of the neutralization level (the neutralization density is the average electron density such that the beam is exactly neutralized, *i.e.*, $d_n = N_p/\pi abs_B = 1.13 \times 10^7$ electrons/cc).

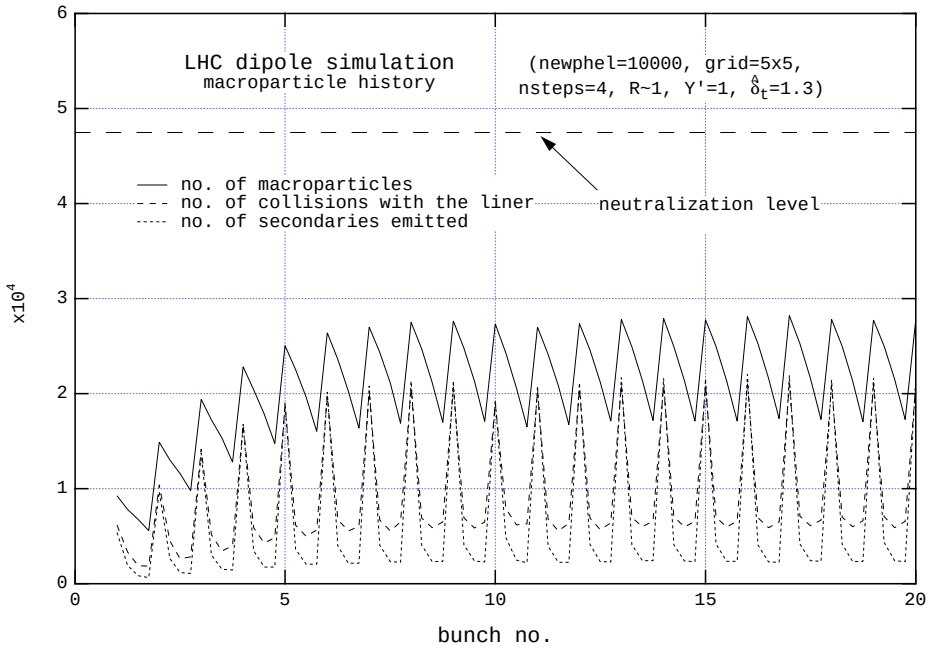

Figure 5: The build-up of the electron cloud as a function of time, measured in bunch passages. The solid line is the total number of macroparticles contained in a given dipole magnet. The dashed line shows the number of macroparticle collisions against the walls of the liner, and the dotted line is the corresponding number of secondary macroparticles emitted from these collisions. The simulation is done for $Y' = 1$ and $\hat{\delta}_t = 1.3$ and is obtained by launching $N_{\rm phel} = 10000$ new photoelectrons per bunch passage. In this case the macroparticle-to-particle ratio is $\mathcal{F} = 4.2 \times 10^6$.

10.2 Dependence of the power deposition on Y' and $\hat{\delta}_t$.

Figure 6 shows the power deposition per unit length in a dipole bending magnet as a function of the photoelectric efficiency Y' for various selected values of the peak SEY, $\hat{\delta}_t$. In his case we have simply taken the curve for $\hat{\delta}(E_0)$ for Al_2O_3 shown in Fig. 4 and scaled its vertical magnitude so that the peak corresponds to the value shown by the labels of Fig. 6. One can see that, for low values of $\hat{\delta}_t$, the power deposition extrapolates to 0 as $Y' \to 0$, as it should. But for $\hat{\delta}_t = 1.8$ the power deposition is substantial even in the limit $Y' = 0$, evidently due to a self-sustaining beam-induced multipacting situation.

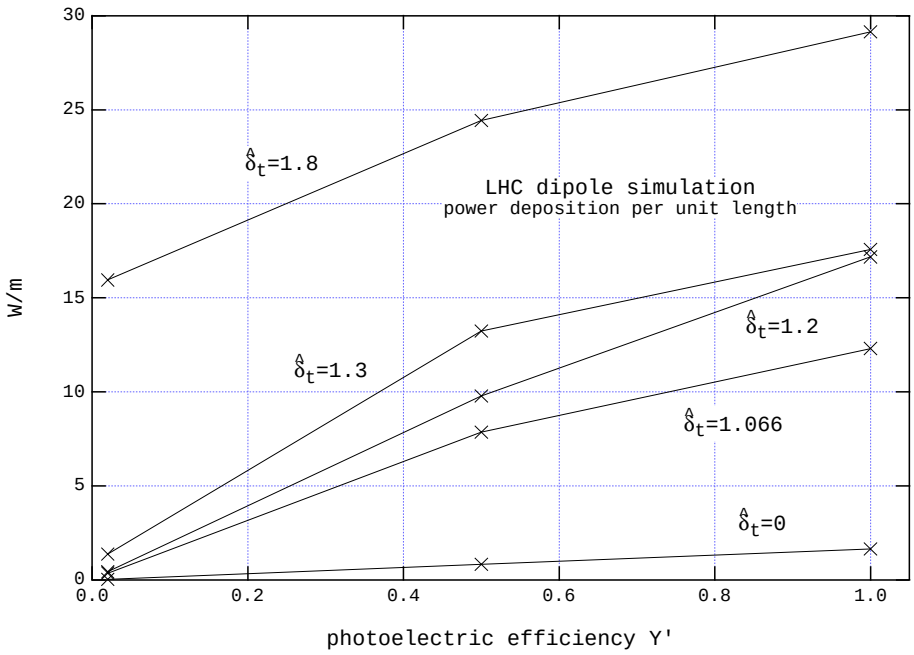

Figure 6: The average power deposition per unit length as a function of Y' for various values of the peak SEY $\hat{\delta}_t$. For sufficiently high $\hat{\delta}_t$ the power deposition is substantial even at $Y' = 0$ due to a self-sustaining beam-induced multipacting condition. The calculation was carried out with $N_{\rm phel} = 100$, a 5×5 grid and 4 steps per bunch spacing.

10.3 Wakes and growth rate.

For the same conditions we have calculated the horizontal and vertical wakes, as shown in Fig. 7. In this case the leading bunch, #10, was displaced by 5 mm in order to generate a wake. One can see that the wake, especially the horizontal, is very short range. By using Eq. (8.3) we find the estimates for the growth rates,

$$\tau_0^{-1} < 0.2 \quad \text{sec}^{-1}, \qquad \text{(horizontal)} \tag{10.1a}$$

$$\tau_0^{-1} \simeq 3.4 \quad \text{sec}^{-1}, \qquad \text{(vertical)} \tag{10.1b}$$

Here the value of the horizontal growth rate is an upper limit because, as is obvious from Fig. 7, we cannot distinguish the actual value of $W(s_B)$ from the background numerical noise.

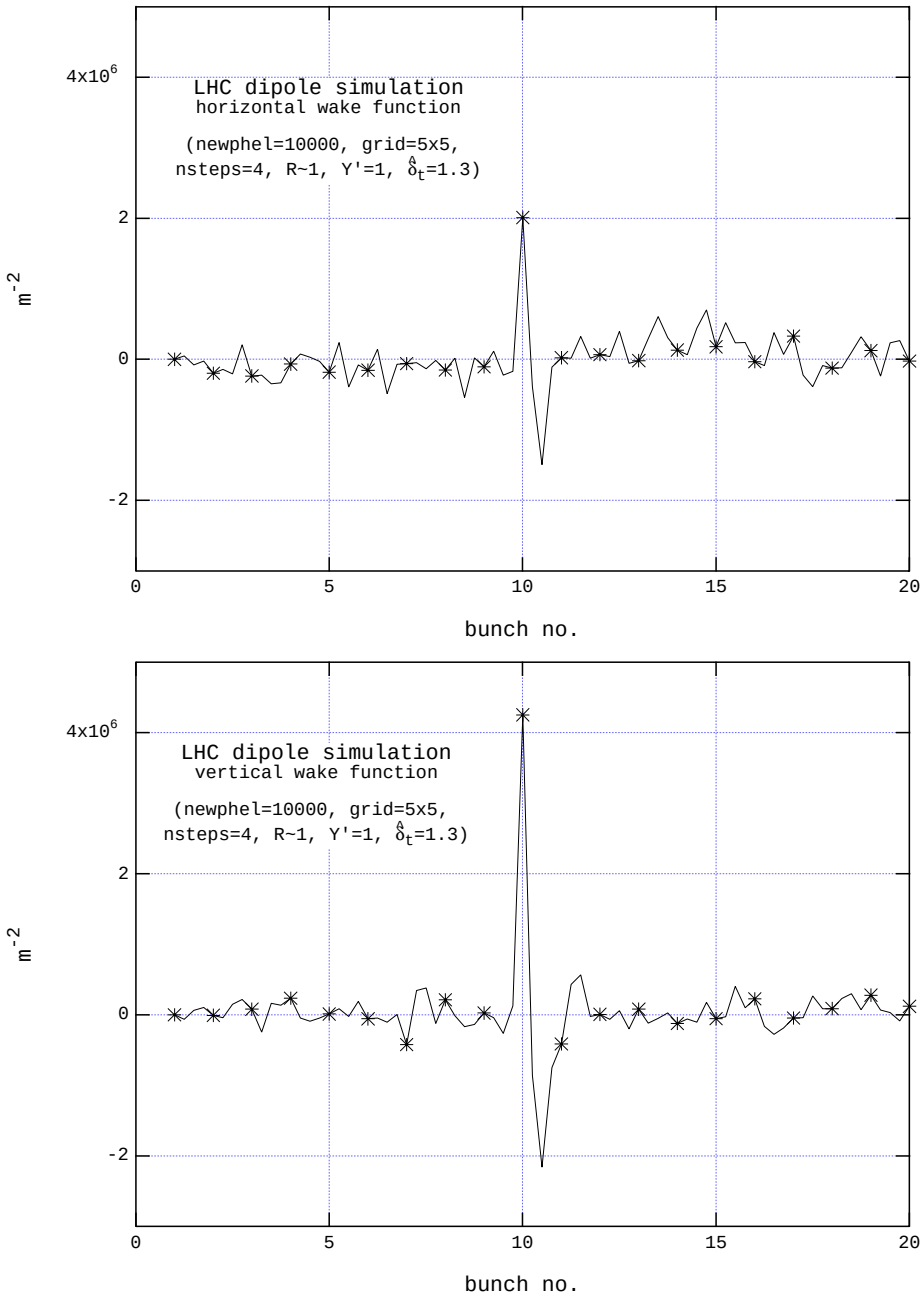

Figure 7: The wake functions for the dipole bending magnets for $Y' = 1$ and $\hat{\delta}_t = 1.3$ obtained by launching $N_{\rm phel} = 10000$ new macro-photoelectrons per bunch passage. The wake functions correspond to the aggregate of all 1232 dipole bending magnets in the ring. Bunch #10 was displaced by 5 mm in order to generate a wake. Ideally, the wake should vanish identically before bunch #10; the fact that it does not is a reflection of the numerical noise of the computation. One can see that the wake is very short range, decaying very quickly after a bunch passage. Asterisks are located at integer intervals, emphasizing the actual bunch locations.

11 Discussion.

As mentioned above, the impulse approximation is not in principle valid for the LHC conditions. We have developed the improved approximation consisting in slicing the bunch, and we have verified that, for the purposes of estimating the power deposition in the LHC dipole bending magnet, the modified impulse approximation given by Eq. (6.2) is approximately valid. Details of this improved calculation will be presented elsewhere [14]. On the other hand, we have not yet carried out such a comparison for the calculation of the wake functions, so the results presented in Sec. 10.3 above are subject to modification. Nevertheless, the results for the growth rates, Eq. (10.1), are in qualitative agreement with those of Zimmermann [2], who does use bunch slicing in his calculations. It should be remembered that other parts of the ring (field-free regions, quadrupole magnets, etc.) will add to the growth rates in Eq. (10.1).

Recently the photoelectric yield and the reflectivity have been measured on a copper surface at $Y' \simeq 0.2$ and $R \simeq 0.8$, respectively [15], for a photon spectrum similar to that expected from the LHC dipole bending magnets. Assuming a peak SEY $\delta_t = 1.3$, which roughly corresponds to copper, these numbers imply a power deposition ~ 5 W/m, which is substantially higher than the value specified in the LHC design [5].

It is therefore important to firm up (or correct) the estimates given here by examining the dependence of the power deposition on the variables that enter the problem. For example, we have assumed here that the photon reflectivity R is close to 1. As mentioned above, this assumption simplifies the calculation substantially by decoupling the beam-electron interaction from the geometrical details of the synchrotron radiation captured by the liner. At the opposite extreme, when $R \simeq 0$, it is easy to see that the power deposition from the electron cloud is very small because the photoelectrons are only generated at the horizontal "edges" of the liner where they remain trapped by the magnetic field (this conclusion assumes that there is no significant self-sustaining beam-induced multipacting condition). It is of obvious interest, therefore, to establish the manner in which the power deposition varies as function of R. Similarly, it is also important to determine its dependence on the shape of the SEY curve, which we have here assumed to correspond to Al_2O_3.

We have also made the assumption that all photons generated by the protons lead to photoelectrons. In fact, some $\sim 50\%$ of the photons have energies below 4 eV and will not, therefore, lead to photoelectrons [14]. If taken literally, this means that our estimate for the power deposition is a factor of 2 too high. To make this conclusion firm, however, one needs to understand the details of the model used to extract the photoelectric yield Y' from the experimental measurements.

12 Acknowledgments.

We are deeply grateful to G. Lambertson for continued collaboration and enlightenment. We are particularly indebted to R. Kirby and F. King for providing data on SEY before publication, to O. Gröbner, N. Hilleret, R. Calder, I. Collins and O. Brüning for many valuable discussions, and to W. Turner, F. Zimmermann, and M. Zisman for valuable comments. We are grateful to NERSC for supercomputer support.

References

[1] Contributions by J. Rogers, M. Izawa and Z. Y. Guo, these proceedings.

[2] F. Zimmermann, "A Simulation Study of Electron-Cloud Instability and Beam-Induced Multipacting in the LHC," LHC Project Report 95, 27 February 1997, and these proceedings.

[3] M. A. Furman and G. R. Lambertson, "The Electron-Cloud Instability in PEP-II: an Update," LBNL-40256/CBP Note-224/PEP-II AP note 97.07,to be published in the Proc. PAC97, Vancouver, BC, May 12–16, 1997.

[4] R. Kirby and F. King, private communication.

[5] "The Large Hadron Collider: Conceptual Design," CERN/AC/95-05(LHC), 20 October 1995.

[6] P. M. Morse and H. Feschbach, *Methods of Theoretical Physics*, McGraw-Hill, 1953, ch. 10.

[7] M. A. Furman and G. R. Lambertson, "The Electron Cloud Effect in the PEP-II Low-Energy Ring," these proceedings.

[8] M. A. Furman, "Compact Complex Expressions for the Electric Field of 2-D Elliptical Charge Distributions," Am. J. Phys. **62**(12), Dec. 1994, pp. 1134–1140.

[9] M. Bassetti and G. A. Erskine, "Closed Expression for the Electric Field of a Two-Dimensional Gaussian Charge," CERN-ISR-TH/80-06.

[10] J. S. Berg, "Energy Gain in an Electron Cloud During the Passage of a Bunch," LHC project note 97, 1 July 1997.

[11] R. W. Hockney and J. W. Eastwood, *Computer Simulation Using Particles*, Inst. of Physics Publishing, 1988.

[12] A. W. Chao, *Physics of Collective Beam Instabilities in High-Energy Accelerators*, John Wiley & Sons, Inc., 1993.

[13] K. Ohmi, "Beam Photo-Electron Interactions in Positron Storage Rings," Phys. Rev. Lett. **75**(8), pp. 1526–1529 (1995).

[14] M. A. Furman, "The Electron-Cloud Effect in the LHC," to be published.

[15] I. Collins, private communication.